Doppler Spread Spectrum of a Circularly Moving Receiver in an Anechoic and a Reverberation Chamber

Myung-Hun Jeong[1, *], Byeong-Yong Park[1], Jung-Hwan Choi[2], and Seong-Ook Park[1]

Abstract—The Doppler phenomena caused by a moving receiver or environmental scatters around a receiver were emulated in an AC (Anechoic Chamber) and a RC (Reverberation Chamber) using platform and mode stirring. In order to verify the emulated Doppler spread spectrum, the measured results in the AC and the RC were investigated by incorporating Jakes's and 802.11 TGn Doppler models, respectively.

1. INTRODUCTION

Doppler spectra are important for determining the time variance of wireless channels and very critical for OFDM (Orthogonal Frequency Division Multiplexing), which is an essential digital modulation method for 4G wireless communication [1, 2]. The usual situation for Doppler phenomena involves a mobile user with moving antennas in a random propagation channel, leading to the classical Jakes' spectrum. Other cases include a stationary user and time-varying channel due to the movements of external scatterers, such as surrounding vehicles and people in indoor and outdoor environments [3, 4], and those cases generally lead to Inverted-V shaped Doppler models.

As a mobile terminal can be exposed to various propagation channels, several types of Doppler phenomena can occur in a mobile communication environment. Traditionally, a base station antenna is always located on a cell phone tower, mast or roof-top for high-quality communication, and it offers a LOS (Line-Of-Sight) propagation channel between the transmitting and receiving antennas [5]. On the other hand, modern mobile applications also work in multipath channels such as urban settings and indoor environments. In order to evaluate the realistic performances of mobile communication systems, it is necessary to characterize the Doppler effect in various propagation channels.

The Doppler effect can be emulated using a channel emulator or several mode stirrers in an AC (Anechoic Chamber) and a RC (Reverberation Chamber) [6, 7]. The Doppler emulation methods in [6] have lower operation cost, a shorter test cycle, and repeatable and reliable measurement conditions compared to OTA (Over The Air) testing in an open area site. In the AC, the channel sounder can emulate a specific fading channel and induce Doppler effects for MIMO OTA testing. The micro Doppler phenomenon can be researched by the dynamic measurement of a micro motion target in the AC [8]. When the Doppler effect is produced by several mode-stirrers in the RC [9], an inverted V- or Bell-shaped Doppler spectra can be obtained, and characterized by specific threshold power [10]. By utilizing a slowly moving mode-stirrer, the heavy Doppler effect can be emulated and analyzed by sampling method [11]. All of the above researches focused on the Doppler phenomena by moving scatters and environmental parameters in an AC and an RC, and none of the cases were specifically characterized by theoretical modeling.

This paper describes the M- and Bell- and Spike-shaped Doppler spread created by a moving receiver and calculates the RMS Doppler bandwidths for precise modeling. In addition, we verify the Doppler phenomena according to different radio wave channels in the AC and the RC by suggesting theoretical modeling.

2. DOPPLER SPREAD AND MODELING

The Doppler spectrum can be obtained by the square of the absolute value of the Fourier transform of the time-variant transfer function. We denote the time-variant transfer function $H(f, t)$ where f and t are frequency and time in the wireless channel. According to the autocorrelation theorem, the autocorrelation, $r_{HH}(f_0, \Delta t)$, of the time-variant function is equivalent to the conjugate of the function's Fourier transform. So the Doppler spread spectrum can be easily obtained using the Fourier transform of the time-variant transfer function, as follows;

$$D_F(f_0, \lambda) = F\{r_{HH}(f_0, \Delta t)\} = F\{E[H * (f_0, t)H(f_0, t + \Delta t)]\}$$
$$= F\{H(f_0, t)\}F\{H * (f_0, t)\} = |F\{H(f_0, t)\}|^2 \qquad (1)$$

where F and E mean the Fourier transform and expectation; superscript $*$, f_0 and Δt represent the complex conjugation, observation frequency, and time difference, respectively.

Because the time-variant transfer function is equal to the $S_{21}(f, t)$ measured with a VNA (Vector Network Analyzer), it can be directly obtained by a VNA at a fixed frequency without taking a channel impulse response.

Originally, the Doppler effect can be caused by a moving TX, RX, or by surrounding objects which move at a greater speed than the TX and RX in various mobile environments. The different wave propagations can be emulated in an AC and an RC. The AC is an unique reference environment for LOS propagation with no reflecting objects. When the receiver moves with a certain speed, a number of components receive from all directions and the channel model can be described for Jakes' spectrum. In the AC, we have only a single-path channel for Jakes' model [12], and the theoretical Doppler spectrum for Jakes' model is shown in (2). That means that the impulse in the frequency domain is spread out across frequencies when TX or RX moves in the mobile communication.

$$S(f) = \frac{1}{\pi f_d^{\max}\sqrt{1 - \left(\frac{f}{f_d^{\max}}\right)^2}} \qquad (2)$$

where $f_d^{\max}$ means the maximum Doppler frequency.

In actuality, mobile systems work in a multipath channel caused by reflection, diffraction, and scattering from surrounding objects, rather than LOS propagation [5]. The Doppler phenomena in multipath fading can be described as the Bell- and Spike Doppler spread in the 802.11 TGn model. In indoor mobile systems, as the TX and RX are stationary and other people are moving around, the environmental Bell-shaped Doppler effect is dominant. Outdoors, the moving user terminal dominantly causes a Doppler effect which has the simple Spike-shape [13]. The RC can emulate these multipath channels in NLOS (Non Line-Of-Sight) propagation using a mode-stirrer, loaded objects and boundary conditions [10, 14]. The Doppler spread of the Bell- and Spike model is as follows;

$$S(f) = \frac{1}{1 + A\left(\frac{f}{f_d}\right)^2} + \frac{B}{1 + C\left(\frac{f - f_{spike}}{f_{spike}}\right)^2} \quad \text{where } f_d = \frac{v_0}{\lambda} \text{ and } f_{spike} = \frac{v_1}{\lambda} \qquad (3)$$

where f_d and f_{spike} are Doppler and spike frequency; v_0 and v_1 are environmental and user terminal speed; λ is the wavelength at the observation frequency.

The first term in Eq. (3) represents the Bell-shape due to moving external scatters, and A is constant to specify the environmental Doppler spread. The second term determines the Spike-shape by a moving user terminal in a factory or hot-spot environment. B represents the ratio between the Spike peak and the maximum of the Bell-shape. C determines the Spike bandwidth.

3. MEASUREMENTS SETUPS AND MEASURED RESULTS

3.1. Measurement Setup in the AC and RC

In order to emulate the Doppler effects for a rotational moving receiver in LOS and NLOS environments, we conducted platform stirring in both the AC and the RC.

The AC emulates reference environments for characterizing Doppler phenomena for LOS communication. Figure 1 shows the geometry of the AC which enables RX circular motion by platform stirring in LOS environments. The dimensions of the AC are $6.0\,\mathrm{m}\,(W) \times 10.0\,\mathrm{m}\,(L) \times 5.0\,\mathrm{m}\,(H)$ and it can be used to measure the far field radiation patterns of the antenna. A double-ridged horn antenna ($0.8 \sim 11\,\mathrm{GHz}$) is used as the TX antenna. The RX antenna is a dipole antenna which has an omnidirectional radiation pattern for WiMAX ($2.5 \sim 2.7\,\mathrm{GHz}$). The RX antenna is mounted on the edge of the platform within the quiet zone and aligned with the same polarization as the TX antenna for achieving LOS propagation.

The RC emulates a multipath channel with rich reflections for testing mobile applications in NLOS communication. The Doppler measurement setup in the RC is described in Figure 2. The sizes of the RC are $1.2\,\mathrm{m}\,(W) \times 1.8\,\mathrm{m}\,(L) \times 1.4\,\mathrm{m}\,(H)$, and a one mode-stirrer and a rotational platform stage are installed along the Z-axis. The fundamental resonance frequency of the RC is about $150.2\,\mathrm{MHz}$ and the LUF (Lowest Usable Frequency) is about $450.6\,\mathrm{MHz}$. The TX antenna, a double-ridged horn antenna, is located behind the mode-stirrer to avoid making LOS components, and the RX antenna is on the edge of the platform stage for circular motion. In the AC and the RC, the diameter of RX rotational movement on the stage is $500\,\mathrm{mm}$, which results in velocity ranging from 0 to $3.77\,\mathrm{km/h}$ with the change from 0 to 40 RPM, in CW (Clock-Wise) and CCW (Counter-Clock-Wise) directions.
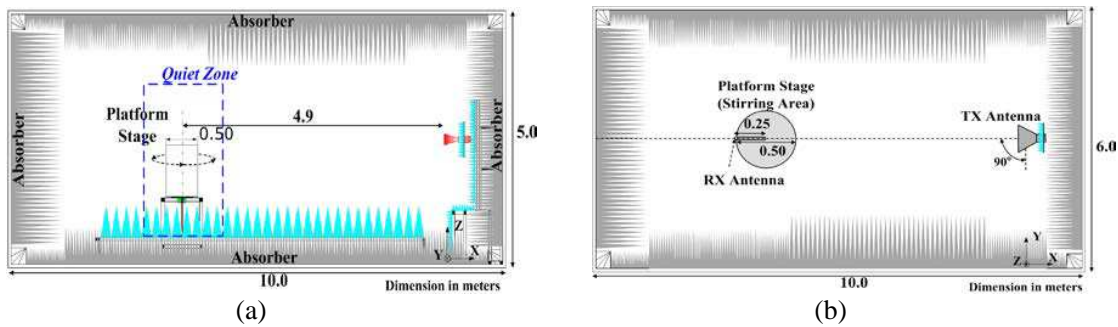
Figure 1. The measurement setup of the AC. (a) The geometries of the AC. (b) The configuration of TX and RX antennas in the AC.
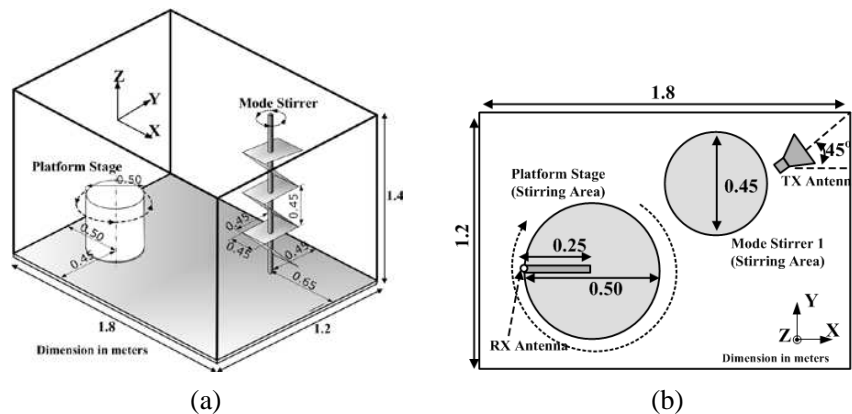
Figure 2. The measurement setup of the RC. (a) The geometries of the RC. (b) The configuration of TX and RX antennas in the RC.

3.2. Measured Results and Discussions in the AC

As mentioned in the previous section, the Doppler spectrum can be obtained by measured S_{21} with a VNA. A network analyzer, Agilent E8357A, was configured in a continuous-wave sweep mode at 2.6 GHz. The total observation time was 20 seconds and the difference in sample acquisition time was 0.025 second, for a total of 801 acquired samples. As the Doppler frequency range is calculated by sampling theory with the time step of sample acquisition, the Doppler spread spectrum can be measured within an observation frequency range from −20 to 20 Hz.

The measured Doppler spread spectra by the rotating RX antenna in the AC are shown in Figure 3. All the measured Doppler spread spectra are normalized to each maximum received power in order to obviously specify the Doppler shape for comparison with each case. To ensure the Doppler phenomena are not influenced by the direction of platform stirring, the measured Doppler spread spectra were obtained for the same rotational movement in opposite directions, CW and CCW. The measured results exhibit reverse symmetry and the calculated RMS Doppler bandwidths in both cases are almost the same. It is induced by that the same phase variations of both cases are the same results. In order to compare the measured results with the ideal Doppler phenomena, we defined Doppler spectrum masks by applying the measured RMS Doppler bandwidth and theoretical Doppler bandwidth to $f_d^{\max}$ of Eq. (2). As the RX antenna moves circularly at a fixed speed, the theoretical maximum Doppler frequency is described in (4).

$$f_d^{\max} = \frac{v}{\lambda} = \frac{1}{\lambda} \cdot \frac{n2\pi R}{60} \tag{4}$$

where λ is the wavelength of the observation frequency, v is the moving velocity which is composed of n and R; RPM (Revolution Per Minute) and radius of circular motion.

As can be seen, the Doppler spectrum in the AC has an M-shape, in that the carrier frequency is spread out with a sharp skirt feature. For some offset values existing outside the range of $f_d^{\max}$, mask 1 for the measured RMS Doppler bandwidth is narrower than the theoretical spectrum, mask 2. The measured spectrum is in good agreement with the theoretical Doppler spectrum, mask 2.

The Doppler spread spectrum is widened with the increasing rotational velocity of the RX antenna; the RMS Doppler bandwidth at 20 RPM is 3.7 Hz and at 10 RPM is 1.8 Hz. This means that the faster moving RX antenna induces more fading due to the heavy phase variations of the received power of the RX antenna.
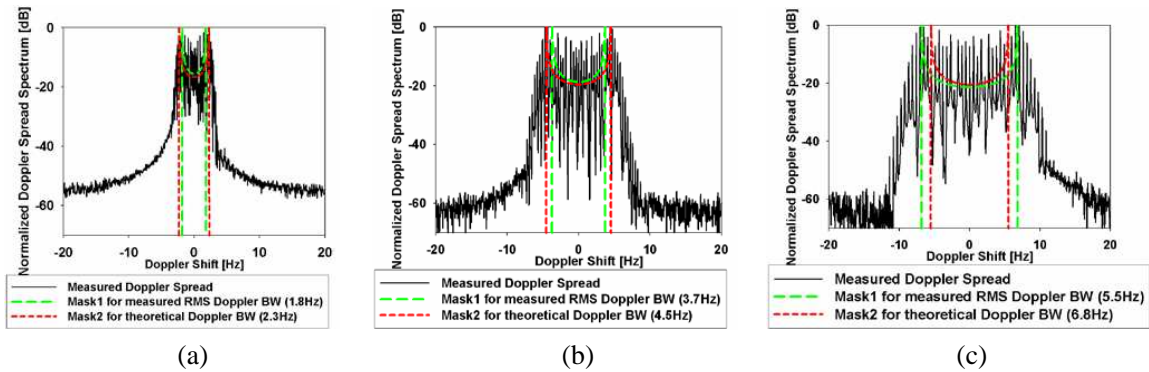
Figure 3. The measured Doppler spread spectrum with platform stirring in the AC. (a) Platform at 10 RPM in CW. (b) Platform at 20 RPM in CW. (c) Platform at 30 RPM in CW.

3.3. Measured Results and Discussions in the RC

The measured Doppler spread spectra with either mode or platform stirring in the RC are shown in Figure 4. The total observation time is 20 seconds and the difference of sample acquisition time is 0.010 second, for a total of 2001 acquired samples. The observation frequency range is from −50 to 50 Hz. Due to the rich scattering including the LOS and NLOS, there are more Doppler components in the RC than the AC, and the measured Doppler spectra are spread out compared to those of the AC.
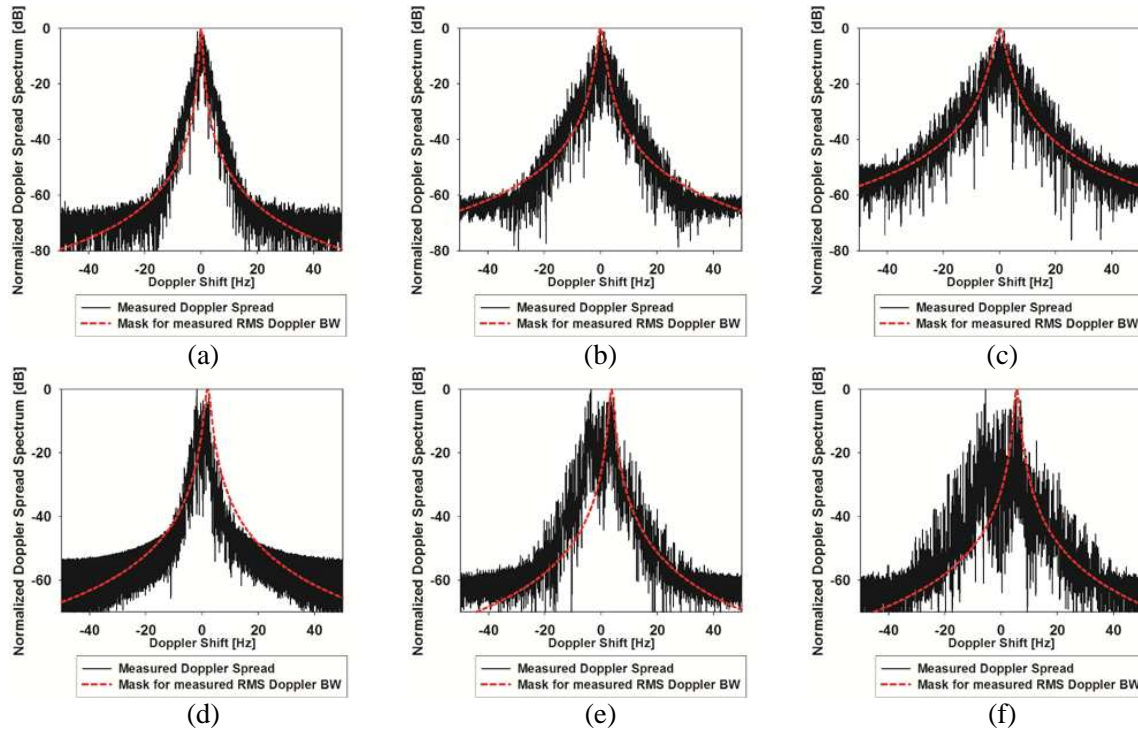
Figure 4. The measured Doppler spread spectrum with either Mode or Platform stirring in the RC. (a) Mode stirrer at 3 RPM in CW. (b) Mode stirrer at 6 RPM in CW. (c) Mode stirrer at 9 RPM in CW. (d) Platform at 10 RPM in CW. (e) Platform at 20 RPM in CW. (f) Platform at 30 RPM in CW.

As shown in [6], there are some environmental Doppler effects caused by rotating a mode-stirrer, and the Doppler spread spectrum is the inverted V- or Bell-shape. For the mode stirrer moving at some rotational velocities in the CW direction, Figures 4(a), (b) and (c) describe the measured Doppler spread spectra and theoretical Doppler mask, Bell model in 802.11 TGn. As mentioned in Section 2, A and f_d, specify the environmental Doppler. In order to obtain the theoretical mask in Figures 4(a)–(c), the calculated RMS Doppler bandwidth in each case is applied to f_d in the first term of Eq. (3); faster mode stirring causes the heavier environmental Doppler. In those three cases, Figures 4(a)–(c), the values of A in Eq. (3) which determine the slope of the spectrum are the same, and the values of f_d increase along with the velocity of the mode stirrer; the RMS Doppler bandwidth of 30 RPM is 4.5 Hz, which is triple that of 10 RPM, 1.5 Hz.

For an RX antenna moving in the CW direction by platform stirring, Figures 4(d), (e) and (f) show the Spike-shape spectra. Similar to the results measured in the AC, the moving velocity of the RX antenna in the RC is reciprocally related with the Doppler effect; the RMS Doppler bandwidth of 30 RPM is almost triple that of 10 RPM. In the second term of Eq. (3), B, C, and f_{spike} determine the Spike-shaped Doppler mask for the moving user terminal. Specifically, the f_{spike} is the measured RMS Doppler bandwidth for a moving RX antenna, which is the reciprocal of the rotating velocity; 2.0, 3.7 and 5.6 Hz in Figures 4(d), (e) and (f). The parameter B in Eq. (3) represents the peak value of the Spike Doppler, so that value in each case is 1. As the Doppler spectrum is spread out when the platform speeds up, parameter C increases with faster rotation.

As the network analyzer excites a sinusoidal wave, there can be a negative Doppler frequency. Thus, to establish some theoretical models for Doppler spectra in the RC, the measured results were fitted to Bell- and Spike Doppler masks at the positive observation frequency, and the coefficients of Eq. (6) are listed in Table 1.

The measured Doppler spread spectra with the combination of circular movement of the RX antenna and mode-stirrer in the RC are shown in Figure 5.

Under the same environmental Doppler effect, the measured Doppler spread spectra using platform

Table 1. Parameters for Doppler mask in Figure 4.

Scenario	Parameters				
	A	B	C	f_d [Hz]	f_{spike} [Hz]
a	8.4			1.5	
b	6.8			3.0	
c	5.5			4.5	
d		1	3.3		2.0
e		1	18.8		3.7
f		1	38.4		5.6

(a)   (b)   (c)

(d)   (e)   (f)
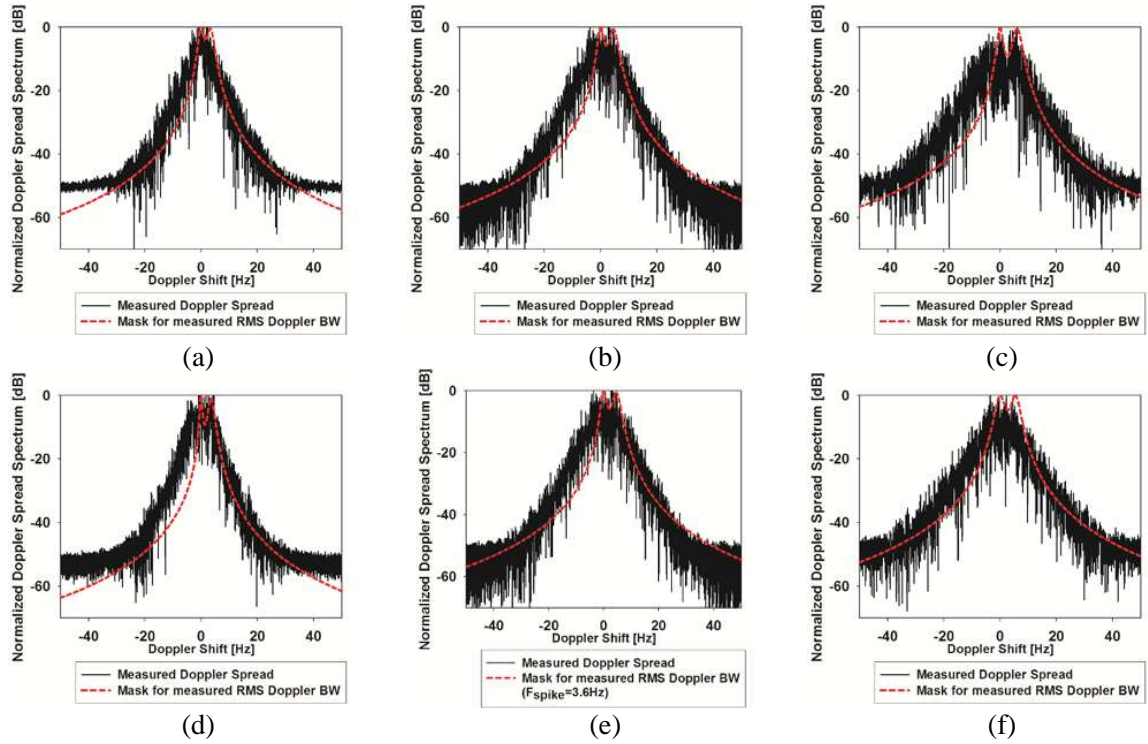
Figure 5. The measured Doppler spread spectrum with either Mode or Platform stirring in the RC. (a) Platform at 10 RPM in CW and Mode stirrer at 6 RPM in CW. (b) Platform at 20 RPM in CW and Mode stirrer at 6 RPM in CW. (c) Platform at 30 RPM in CW and Mode stirrer at 6 RPM in CW. (d) Platform at 20 RPM in CW and Mode stirrer at 3 RPM in CW. (e) Platform at 20 RPM in CW and Mode stirrer at 6 RPM in CW. (f) Platform at 20 RPM in CW and Mode stirrer at 9 RPM in CW.

stirring up to 30 RPM in the CW direction are described in Figures 5(a), (b) and (c). In those cases, the other measurement setups are the same procedure as in Figure 4(b); the mode stirrer moves at 6 RPM in the CW direction. The measured Doppler spreads in Figures 5(a)–(c) are Bell- and Spike-shape induced by moving scatter and user terminal. As the environmental Doppler effect is fixed, the Bell shapes in Figures 5(a)–(c) are applied by the Bell Doppler model in Figure 4(b). Therefore the parameters A and f_d in the theoretical masks of Figures 5(a)–(c) are the same as those values of Figure 4(b). In Figure 5, the peak values of the Spike Doppler are the same as those of the Bell Doppler, so all the parameters B are 1. As the envelopes of the Spike spectra have steep slopes compared with Figures 4(d)–(f) just for the moving user terminal, parameters C of the theoretical masks have lower values than Figures 4(d)–(f). With faster platform movements, the more the Doppler phenomenon occurs for a moving RX antenna;

the calculated RMS Doppler bandwidth, which is applied to f_{spike} in the second term of Eq. (3), in Figure 5(c) has increased more than in Figure 5(a).

Figures 5(e)–(f) describe the Doppler spreads according to the environmental Doppler, generating from the mode-stirrer, when the RX antennas rotate with the same velocities. In those cases, the other measurement setups are the same procedure as Figure 4(e); the RX antenna moves at 20 RPM in the CW direction. The measured Doppler spreads in Figures 5(d), (e) and (f) are Bell- and Spike-shape, like the measured results of Figures 5(a)–(c). With a faster mode stirrer, the more environmental Doppler effects occur for the moving RX antenna; when the mode stirrer speeds up in Figure 5(f), the environmental Doppler effect is increased more than in Figure 5(e). As the moving RX antenna is influenced by the mode stirrer, the Spike-shaped Doppler is modified by environmental scatter; f_{spike} is increased and C, Spike bandwidth, is decreased, compared with those of Figures 4(d)–(f). From these results, it is clear the various Doppler phenomena for mobile terminals can be emulated in the RC, and the measured Doppler spectra in the RC are in good accord with the Bell- and Spike-shaped Doppler models. Table 2 describes how the coefficients of Eq. (6) establish some theoretical models for the Doppler spectra in Figure 5.

Table 2. Parameters for Doppler mask in Figure 5.

Scenario	Parameters				
	A	B	C	f_d [Hz]	f_{spike} [Hz]
a	6.8	1	5.3	3.0	3.4
b	6.8	1	6.4	3.0	4.6
c	6.8	1	11.1	3.0	6.1
d	8.4	1	7.2	1.5	3.6
e	6.8	1	6.4	3.0	4.6
f	5.5	1	8.4	4.5	5.5

4. CONCLUSIONS

Various Doppler phenomena were investigated by rotating a receiver or mode-stirrers, while user terminals did not actually move away. The Doppler effects caused by platform stirring in both CW and CCW directions were the same, having the same phase variations in the reverse order. The Doppler phenomena were proportional to the rotational velocity of the RX antenna because the phase variations of circular motion induced the fading channel. The Doppler spread spectra measured in the AC can be specified by Jakes' Doppler model, which describes the Doppler phenomena caused when a receiver moves alone in a LOS propagation channel. Unlike the RC, the Doppler effect for just platform stirring was fitted with a Spike-shape, the moving user terminal scenario, while with the moving mode-stirrer it was specified by the Bell-shape, surrounding external scatter scenario, in NLOS propagation.

ACKNOWLEDGMENT

REFERENCES

1. Rugini, L. and P. Banelli, "BER of OFDM systems impaired by carrier frequency offset in multipath fading channels," *IEEE Trans. Wirel. Commun.*, Vol. 4, No. 5, 2279–2288, 2005.
2. Lee, Y. D., D. H. Park, and H. K. Song, "Improved channel estimation and MAI-robust schemes for wireless OFDMA system," *Progress In Electromagnetics Research*, Vol. 81, 213–223, 2008.

3. Andersen, J. B., J. O. Nielsen, G. F. Pedersen, G. Bauch, and G. Dietl, "Doppler spectrum from moving scatterers in a random environment," *IEEE Trans. Wirel. Commun.*, Vol. 8, No. 6, 3270–3277, 2009.

4. Ma, B.-K., L.-X. Guo, and H.-T. Su, "Statistical characteristics of the multi-path time delay and Doppler shift of a radar wave propagating through the Ionosphere," *Progress In Electromagnetics Research*, Vol. 138, 479–497, 2013.

5. Kildal, P. S., "OTA measurements of wireless stations in reverberation chamber versus anechoic chamber: From accuracy models to testing of MIMO systems," *2010 International Workshop on Antenna Technology (iWAT)*, 1–4, 2010.

6. Wright, C. and S. Basuki, "Utilizing a channel emulator with a reverberation chamber to create the optimal MIMO OTA test methodology," *2010 Global Mobile Congress (GMC)*, 1–5, 2010.

7. Hallbjorner, P. and A. Rydberg, "Maximum Doppler frequency in reverberation chamber with continuously moving stirrer," *2007 Antennas and Propagation Conference, LAPC 2007*, 29–232, Loughborough, 2007.

8. Liu, J., G. Li, L. Ma, W. Hu, Y. Li, and X. Wang, "Dynamic measurement of micro-motion targets in microwave anechoic chamber," *2009 IET International Radar Conference*, 1–4, 2009.

9. Chen, X., "Evaluation and measurement of the Doppler spectrum in a reverberation chamber," *Progress In Electromagnetics Research M*, Vol. 26, 267–277, 2012.

10. Choi, J. H., J. H. Lee, and S. O. Park, "Characterizing the impact of moving mode-stirrers on the Doppler spread spectrum in a reverberation chamber," *IEEE Antennas Wirel. Propag. Lett.*, Vol. 9, 375–378, 2010.

11. Karlsson, K., X. Chen, P.-S. Kildal, and J. Carlsson, "Doppler spread in reverberation chamber predicted from measurements during step-wise stationary stirring," *IEEE Antennas Wirel. Propag. Lett.*, Vol. 9, 497–500, 2010.

12. Jakes, W., *Microwave Mobile Communications,* Wiley & Sons, 1975.

13. "IEEE 802.11-03/940r4: TGn channel models," IEEE, 2004.

14. Chen, X., P. S. Kildal, and J. Carlsson, "Determination of maximum Doppler shift in reverberation chamber using level crossing rate," *Proceedings of the 5th European Conference on Antennas and Propagation (EUCAP)*, 62–65, 2011.